New Operando IR Technique to Study the Photocatalytic Activity and Selectivity of TiO 2 Nanotubes in Air Purification: Influence of Temperature, UV Intensity, and VOC Concentration

Mohamad El-Roz, Monika Kus, Pegie Cool, Frederic Thibault-Starzyk

New operando-IR technique to study the photocatalytic activity and selectivity of TiO_2-nanotubes in air purification: influence of temperature, UV intensity and VOCs concentration.

Mohamad El-Roz*[a], Monika Kus[b], Pegie Cool[b], Frederic Thibault-Starzyk[a]

**Corresponding authors: mohamad.el-roz@ensicaen.fr*

[a]Laboratoire Catalyse et Spectrochimie (LCS), *ENSICAEN, Université de Caen, CNRS* , 6, Bd du Maréchal Juin, 14050 Caen Cedex, France. Fax: *+33 (0)231 45 28 22*, Tel: *+33 (0)231 45 27 32* , E-mail: mohamad.el-roz@ensicaen.fr

[b] *Laboratory of Adsorption and Catalysis, Department of Chemistry, University of Antwerpen, Universiteitsplein 1, B-2610 Wilrijk, Belgium.*

Abstract

The photooxidation of methanol, n-hexane and carbon monoxide using TiO_2-nanotubes (TNTs) has been investigated by a new IR-operando technique. Following the photocatalytic reaction by time resolved IR spectroscopy coupled with mass spectrometry (MS) allowed a surface study of the photocatalyst with on line analysis of the products. The identification of the species adsorbed on the photocatalyst surface and those detected in the gas phase led to further clarify the photooxidation mechanisms. The characterization of the photocatalyst has been performed by IR, Raman, UV-visible, XRD, N_2-sorption, SEM and TEM techniques. The activity and selectivity of the photocatalyst have been determined by quantitative studies using gas-IR and MS. For comparison, photooxidation reactions, using TiO_2-P25 as reference, have been performed under the same conditions. The influence of different parameters such as temperature, VOC concentrations and UV irradiation intensities on the reactivity and selectivity of the photocatalytic reaction has been investigated. The

temperature effect has been shown by TPD measurements (from RT to 200°C). The TNTs material showed a higher reactivity and CO_2-selectivity in comparison with TiO_2-P25.

Keywords: TiO_2 nanotubes, Photocatalysis, operando-IR, VOC and carbon monoxide photooxidation, temperature and VOC concentration effect.

Introduction

The decontamination of air in closed spaces such as aircrafts, air-conditioned spaces, *etc*..., from volatile organic contaminants/compounds (VOC) attracts special attention due to its economic and health interests. The use of heterogeneous catalysts, largely employed for the control and treatment of exhaust gases, presents one of the key features for such treatment. Indeed, the reaction on the catalyst can be induced either by heating, or by UV light when using a photocatalyst. This latter presents many advantages such as low cost and low environmental impact, and TiO_2 is considered as the most promising catalyst for this purpose. TiO_2 is cheap, resistant to photocorrosion, photostable and non toxic. It is easy to prepare, environmentally friendly and has a low band gap energy.[1,2,3] With new environmental issues, it is expected that applications for TiO_2 will grow with a high speed. In particular, the improvement of TiO_2 activity in organic photodegradation processes is needed for large scale industrial treatment processes such as waste water treatment and de-VOCs[4,5,6]. Titania nanotubes (TNTs) have been proven to be highly promising for potential applications in various fields[7,8]. Titania nanotubes layers were shown recently to be more efficient in the photocatalytic conversion of organic azo dyes than common photocatalysts [4,9]. In the present work, TiO_2-nanotubes (TNTs) have been prepared by a hydrothermal method according to S. Ribbens et al.[10], and studied in the photooxidation of methanol, n-hexane and carbon monoxide by a new operando IR technique. The common point of the air pollutants chosen (CH_3OH, C_6H_{14} and CO) is their toxicity even at low concentration. The comparison of

methanol and n-hexane photooxidation allows investigating the influence of hydrophilic/hydrophobic ratio and hydrocarbon chain length on the photooxidation activity. In order to estimate the activity of TNTs in gas phase photooxidation reactions, a well known photocatalyst, TiO_2-P25 from Degussa, has been used. The influence of various parameters, such as the temperature, the UV irradiation intensity and the concentrations of VOCs or CO was studied in real time. The present work shows the interest of operando IR to perform photocatalytic studies, on self supporting wafers of the catalysts and in gas flow in conditions very close to those of the real reaction.

Experimental part

Synthesis

Titanium based nanotubes were synthesised using a hydrothermal method. In a typical preparation 4,5g of commercial TiO_2 powder was dispersed in 80ml of 10M NaOH solution under vigorous stirring. The mixture was stirred for 1 hour and transferred to an autoclave with internal volume 150ml, followed by hydrothermal treatment at 150˚C for 48 hours. After 48 hours the autoclave was quenched to room temperature and the product was recovered by centrifugation. The precipitation was washed 3 times with distilled water. Afterwards the wet cake was dispersed in 240ml of 0,1M HCl solution and stirred for 30 min. H-tubes were recovered by centrifugation and washed until the pH reached 1. The precipitate was washed 3 times with distilled water and 2 times with ethanol. The product was calcined at 350˚C for 6h to obtain mixed phase nanotubes.

Characterisation

X-ray diffraction

In order to investigate the crystallinity and phase purity of the samples, calcined and as-synthesized TiO_2-nanotubes crystals have been characterized, and compared to TiO_2-P25 and TiO_2-rutile (99.9% of purity), by X-ray diffraction (XRD) on a PANanalytical (X-Pert Pro) diffractometer with CuKα1 source (λ=0.15406 nm, 40 kV, 30 mA).

SEM and TEM

The morphological features and the chemical analyses of the samples were studied using Scanning Electron Microscope (SEM, Hitachi S3460) and Transmission Electron Microscope (TEM, Phillips CM 20) operating at 200kV.

Nitrogen sorption

Nitrogen sorption measurements of TiO_2 samples were carried out at -196°C on a Micromeritics ASAP 2020 micropore analyse. The samples were degassed at 150°C K for 24 h. Surface areas were calculated using BET equation.

UV-vis DR

UV-Vis DR measurements were performed on Thermo-electron evolution 500 UV-Vis spectrometer equipped with RSA-CU40 Diffuse Reflectance cell. From UV-Vis DR spectra information over the band gap energy can be obtained.

Raman

Raman spectra were recorded on a Nicolet Nexus FT-Raman spectrometer with an InGaAs detector and a 1064 nm Nd:YAG laser

Acidic properties

The acidic properties of the resulting materials were investigated by temperature desorption (TD) of pyridine followed by IR. Powders were pressed (~10^7 Pa) into self-supported discs (2 cm^2 area, 9-10 $mg.cm^{-2}$) and placed in an IR cell equipped with KBr windows. IR spectra have been recorded using a Nicolet 6700 IR spectrometer equipped with a MCT detector and an extended-KBr beam splitter. Spectra were recorded in the 400-5500 cm^{-1} range at 4 cm^{-1} with 128 scans. A movable quartz sample holder allowed placing the self-supported discs in the infrared beam for recording spectra, and moving it into a furnace at the top of the cell for thermal treatment.[11] Pyridine (Py) adsorption was performed by introduction of doses inside the infrared cell containing the previously activated (under vacuum at 200°C for 5 h) self-supported discs. After introduction of each dose of Py, the samples were heated at 200°C for 10 min to allow diffusion toward all accessible sites before recording the spectrum. Infrared spectra were recorded after Py saturation (1.33 mbar at equilibrium) followed by evacuation at 200°C to remove physisorbed species. In all experiments, analytical grade pyridine (Aldrich) was used after water trapping with molecular sieve 3A. The calculation of the IR band surface area has been performed using Omnic v8.2 software. The values were normalized for the same samples weight (20 mg).

Conditions for Photocatalytic operando test

The photocatalytic oxidation of methanol has been followed by IR spectroscopy. The powder of the desired catalyst was pressed into self-supported wafers (Ø = 16 mm, m~10 mg/cm^2). IR spectra were collected with a Nicolet 5700 FT-IR spectrometer (64 scans/spectrum) equipped with a MCT detector. The operando system is connected to a flow set-up. Gases are introduced into the lines (heated at 60°C) by mass flow controllers. The two gas mixtures, so called “activation” and “reaction” flows, can be prepared and sent

independently to the reactor cell. The “Sandwich” reactor-cell used in this study is an evolution of the *operando* cell developed by Saussey et al.[12], which has proven its reliability over many years of *operando* studies [12,13]. It is made of a stainless steel cylinder that carries a toroidal sample holder in its centre, where the catalyst self supporting wafer is placed. Tightness is obtained by Kalrez© O-rings, and the dead volume (typically defined as the residual space between each sample face and the windows) is reduced to about 0.4 ml by filling the empty space with KBr windows placed on each side of the sample holder. The surface analysis is made possible without superposition of the gas phase signal and fluid dynamics is very similar to that inside a honeycomb monolith. Gases are introduced on the sample by 1/8" OD pipe and collected on the opposite side of the sample holder. More details can be found in the following references[14,15]. For this specific photocatalytic oxidation study, UV irradiation was carried out with a polychromatic light of a Xe-Hg lamp (LC8 spot light Hamamatsu, L10852, 200 W). It has been performed by using a UV-light guide (A10014-50-0110) mounted at the entrance of modified IR operando cell as presented in Scheme 1 in order to establish a “homogeneous” irradiation. UV irradiation intensity (I_0) has been measured using a light power meter (from Hamamatsu).

In such a configuration, at atmospheric pressure, and small amounts of VOC to be removed, a low partial pressure of VOC was established using a saturator at a carefully controlled temperature. The gas mixture composition was then fixed at 0.01 to 0.5 vol.% methanol, n-hexane or CO, 20 vol.% O_2 in Ar and the total flow was adjusted to 25 cm^3/min. The analysis of the outlet gases was performed by means of a Pfeiffer Omnistar mass spectrometer. Likewise, FT-IR spectra of the gas phase were collected using a gas microcell.

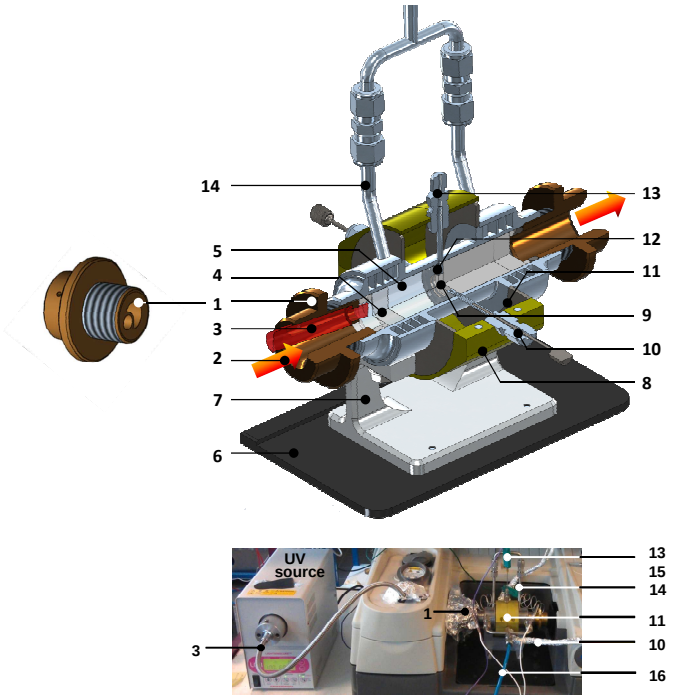

Scheme 1. The "sandwich" reactor-IR cell modified for studying UV photocatalysis. (1) Adjusting nut for airtightness (modified for UV-guid position), (2) IR beam, (3) UV-light guid, (4) Kalrez O-ring, (5) KBr windows, (6) Spectrometer base-plate, (7) IR cell support, (8) Oven location, (9) Sample (wafer), (10) Gas inlet, (11) External shell, (12) Wafer holder, (13) Thermocouple location, (14) Air cooling outlet, (15) Gas outlet, (16) Air cooling inlet.

Photooxidation reaction at RT where performed after a photoactivation at RT under 20%O_2/Ar. Photooxidations at variable temperature were carried out after activation of the pellet at 200 C for two hours.

The photooxidation of methanol (MeOH) has been performed using TiO_2-P25 and TNTs as photocatalyst under the same conditions (concentration, temperature, flow rate…). The concentration was fixed at 5040 ppm of MeOH in 20% O_2 in Ar at 25 cm^3/min. The UV intensity (I_0) was estimated to ~2 mW/cm^2 (~20% of the lamp intensity).

Results and discussion

Characterization

The nanomorphology of calcined TiO_2 nanotubes (TNTs) is confirmed using scanning electron microscope (SEM) and transmission electron microscopy (TEM). The results are presented in Figure 1. The average length of the tubes was found around 90 nm.

< Figure 1 here>

Figure 2 presents the X-ray diffraction patterns of TiO_2-rutile, TiO_2-P25, as synthesized and calcined TNTs. The results show that X-ray diffraction patterns of TNTs correspond to TiO_2 anatase phase and no significant modification has been observed after calcination. The broadening of X-ray peaks observed, in comparison with TiO_2-P25 could be assigned to the nanocrystalline nature of the TNTs nanotubes. Moreover, after calcination at 350°C, no rutile phase has been observed. For reasons of comparison also the XRD pattern of rutile phase is reported in Figure 2.

< Figure 2 here>

Raman spectra are presented in Figure 3. Spectra of the calcined sample are compared to the spectra of the sample before calcination. The peaks at Raman shifts 188, 273, 369, 449 and 663 cm^{-1} reveal the presence of a trititanate structure for the non-calcined form. After the calcination process at 350˚C peaks at 399, 510 and 639 cm^{-1} are appearing which are characteristic for the anatase form of TiO_2. This indicates that the sample undergoes incomplete transformation from $H_2Ti_3O_7$ to anatase TiO_2 during the calcination procedure.

< Figure 3 here>

The N_2-sorption results show a surface area of TNTs (230 m^2/g) 4 times higher with respect to TiO_2-P25 (55 m^2/g) (Figure 4). The hysteresis present at 0.8 to 0.9 in the case of TNTs assigned to the textural porosity of this nanotube.

< Figure 4 here>

The photocatalytic activity of a material is determined by the band gap energy, defect sites and surface area of the sample. Band gap energy can be calculated from UV-Vis DR spectra. In Figure 5 spectra of TiO_2-P25 (a), TiO_2-nanotube after calcination (b) and TiO_2-nanotube before calcination (c) are compared. The band gap energies for the samples are respectively 3.07, 3.21 and 3.27eV. TiO_2-P25 sample has lower band gap energy than the prepared nanotube samples. According to the literature, this slight difference could be assigned to the TiOH content and Ti(III)/Ti(IV) ratio present in the different samples which could affect the TiO_2 band gap values.[16] The photocatalytic activity depends also on the surface area which is much higher for the TiO_2-nanotube samples.

< Figure 5 here>

Acidic properties

The IR spectra (collected under dry air at room temperature) showed that the water content (calculated using the band at 1630 cm^{-1}) is about three times higher in TNTs than in TiO_2-P25. After activation under vacuum at 200°C, the IR spectra showed too separate bands at ~3720 cm^{-1} and ~3670 cm^{-1} (Figure 6) assigned to Ti(III)OH and Ti(IV)OH respectively[17,18]. The TiOH band area is twice higher in TNTs material which explains the higher hydrophilicity of this photocatalyst in comparison to TiO_2-P25.

< Figure 6 here>

The IR spectra of the photocatalyst surfaces after pyridine adsorption, and evacuation at 200°C under vacuum (~10^{-6} mbar), are presented in Figure 7. New bands appeared at 1610, 1575 and ~1445 cm^{-1}, assigned to pyridine molecules (Py) adsorbed on Lewis acid centers (Ti cation sites), and at 1490 cm^{-1}, assigned to Py on Brønsted (Py-B) and/or Lewis (Py-L) acidic sites[19]. The bands at 1610 cm^{-1} and 1445 cm^{-1} are assigned to pyridine molecules chemisorbed by the interaction between the nitrogen lone pair and the substrate surface[19,20,21]. Table 1 summarizes the area of Py-B and Py-L bands. More Py was adsorbed on the TNTs than on TiO_2-P25 surface (1.5 to 2.5 times), possibly because of the higher amount of TiOH on TNTs (Figure 6). Looking at the intensities for the OH bands, the $Ti(III)OH_{(TNTs)}$/ $Ti(III)OH_{(TiO2\text{-}P25)}$ ratio was about 1.3, close to the ratio of the area of the band at 1610 cm^{-1} (1.4) on the two solids. For $Ti(IV)OH_{(TNTs)}$/ $Ti(IV)OH_{(TiO2\text{-}P25)}$ (band at 3670 cm^{-1}), a value of 2.6 has been found, close to that obtained for the area of the band at 1448 cm^{-1} (2.5) on the two samples (Table 1). This indicates that the bands at 1610 and 1448 cm^{-1} could be assigned to pyridine molecules adsorbed on Ti(III)OH sites and on Ti(IV)OH sites, respectively. A thermo desorption would be useful to confirm this hypothesis, but it is unfortunately not possible due to the degradation of pyridine on TiO_2 surface at T>225°C (coke formation on TiO_2 surface has been observed at high temperature). On the other hand the evolution of OH peak height, on TNTs sample, after pyridine adsorption at different temperatures has been followed (Figure 7B). The result shows an increase of the band at 3720 cm^{-1} assigned to pyridine desorption. A slow decrease of the band at 3670 cm^{-1} was observed, assigned to coke formation. This is in good agreement with a lower acidity for Ti(III)OH than for Ti(IV)OH sites.

< Figure 7 here>

< Table 1 here>

Methanol photooxidation

Photooxidation reactivity and temperature effect

The IR spectra of TNTs during methanol adsorption are presented in Figure 8A. A decrease of the band at 3820-3600 cm^{-1} is observed (ν(TiO-H) vibration mode), simultaneously with an increase of a broad band at 3660-3000cm^{-1}, assigned to the vibration band of H-bonded TiOH (methanol adsorption on TiOH). Figure 8B shows the IR spectra of TiO_2-P25 and TNTs samples monitored at RT after saturation with methanol (MeOH) before UV irradiation. Four main bands are observed between 3000 and 2700 cm^{-1} assigned to CH_3 (methanol) vibration modes. The bands at 2920 and 2820 cm^{-1} correspond respectively to the $\nu_s(CH_3)$ and $\nu_{as}(CH_3)$ vibration modes of dissociatively chemisorbed methanol (with rupture of the O-H bond) on TiO_2 surface[22,23,24]. The relatively high intensity of these two bands on TNTs compared to those on TiO_2-P25 shows a high methanol chemisorption on TNTs surface (in agreement with the high amount of Ti(IV)OH sites on this material). The additional bands situated at 2945 and 2840 cm^{-1} are attributed to $\nu_s(CH_3)$ and $\nu_s(CH_3)$ vibration modes of methanol molecularly adsorbed on TiO_2 surfaces[22,23,24].

< Figure 8 here>

Figure 9 shows the IR spectra vs. time (and temperature) for the gas phase during the photooxidation of methanol on TNTs (A) and TiO_2-P25 (B) as photocatalysts. It shows a spontaneous decrease of methanol bands after UV irradiation. New bands appearing during the photooxidation were assigned to CO_2 (2400-2200 cm^{-1}), -C=O (1820-1670cm^{-1}) and C-H

vibration modes (1275-1100 cm^{-1})[25]. The IR-gas spectra during photooxidation (at RT) are presented in Figure 10. IR spectra of formaldehyde, methylformate and formic acid are also presented, and show that carbonyl species could be a mixture of the three: the CH band at 1275-1100 cm^{-1} assigned to *r*(CH) vibration mode is not present in the case of pure formaldehyde[26]. The quantification of carbonyl species is not possible due to the overlapping IR bands.

< Figure 9 here>

< Figure 10 here>

The quantification of methanol has been performed using the area of the 1090-950 cm^{-1} band assigned to the ν(C-O) vibration mode of methanol. Methanol conversion has been estimated with the following formula:

$$Conversion(\%) = \frac{(A_0 - A_{t(T)})}{A_0} \cdot 100\%$$

with:

A_0= the band area of MeOH (in the gas phase) before photooxidation

$A_{t(T)}$= the band area of MeOH during photooxidation at time "t" (or at Temperature "T")

The selectivity of MeOH transformation to CO_2 has been calculated using the band area of CO_2 measured during a complete and total photocombustion of 5040 ppm of MeOH under special irradiation conditions (I_0=11 mW/cm^2): photocombustion is then 100 % selective (CO_2 production) and the observed band area corresponds to ~5000 ppm of CO_2. This result has been used for estimating CO_2 concentration during the photooxidation of 5040 ppm MeOH under different conditions. The CO_2-selectivity has been calculated as follows:

$$CO_2 - selectivity(\%) = \frac{n_{CO_2}}{n_{MeOH-converted}} \cdot 100\%$$

with:

n_{CO_2} = amount of CO_2 produced in mole.

$n_{MeOH-converted}$ = amount of methanol converted in mole.

Figure 11 illustrates the effect of temperature on methanol conversion and CO_2 selectivity in the case of TNTs (Figure 11-A) and TiO_2-P25 (Figure 11-B). TNTs are 1.5 to 2 times higher compared to TiO_2-P25, with higher CO_2-selectivity (~1.5 times more, see Table 2). The increase of temperature led to an increase of methanol conversion with a maximum at ~180°C (Figure 11). Experiments have been performed at less than 200°C in order to prevent the transformation of the TiO_2 phase, especially in the case of TiO_2-P25, as mentioned in the literature. A decrease in CO_2 selectivity (from 85% to 60%) on TNTs has been observed at T>35 °C, with a plateau at ~60 % for T>90°C. For TiO_2-P25, no significant effect of the temperature on CO_2 selectivity was observed. The small time lag between CO_2 detection and methanol conversion (~1 min) is assigned to the ignition of methanol desorption from TiO_2 surface leading to a momentary increase of methanol in the gas phase. This is confirmed by the IR spectra of TiO_2 before and during methanol photooxidation when significant decrease of adsorbed methanol has been observed immediately upon switching UV-irradiation on.

< Figure 11 here>

In order to confirm these results, methanol conversion has been calculated using the MS signal for methanol before and during irradiation:

$$Conversion(\%) = \frac{\left(I_0 - I_{t(T)}\right)}{I_0} \cdot 100\%$$

with:

I_0= the MS intensity of m/z=31 signal detected by MS before photooxidation

$I_{t(T)}$= the MS intensity of m/z=31 signal detected by MS during photooxidation at time t (or temperature T).

In addition, the MS signal for H_2O at m/z=18 and for CO_2 at m/z=44 (amplified 5 times) are presented in Figure 12. The results confirmed those obtained by gas-IR: methanol conversion and CO_2 production increased 1.5 to 2 times on TNTs in comparaison to TiO_2-P25 (Figure 12).

< Figure 12 here>

Concentration effect

In order to highlight the concentration effect on methanol photooxidation, 2000 ppm of methanol were sent under the same conditions on TNTs. The gas-IR and MS results are presented in Figure 13. Photooxidation activity was higher than with 5040 ppm of methanol. The CO_2 selectivity is also higher and reached 100% for T>90°C, possibly because of an increase of the Oxidant-species/methanol ratio due to the decrease of methanol concentration.

< Figure 13 here>

Figure 14 presents the IR spectra of TNTs (and the gas phase of the reaction) before and during the photooxidation at RT and at 120°C. After UV irradiation new bands appeared at 2870, 1715, 1650, 1560 and 1370 cm^{-1}. The bands detected at 2870, 1560 and 1370 cm^{-1} are assigned respectively to ν_s(CH), ν_{as}(COO) and ν_s(COO) vibrations of bidentate formate species adsorbed on the catalyst surface. Those observed at 1715 and 1650 cm^{-1} are assigned to ν(C=O) vibrations of formic acid (or methylformate) hydrogen bonded and co-ordinately bonded to Lewis acid sites, respectively[13,25,26,27] (the IR spectra vs. time and temperature during photooxidation of methanol at different temperature are presented in Figure I in the supplementary materials). The IR band at 1570 cm^{-1} reached a maximum at 120°C which means that the temperature favours the formation of bidentate formate, thus explaining the increase of methanol photooxidation. These results suggest that the bidentate formate ions are common intermediates and that the photooxidation mechanism could be presented as follows:

$$TiO_2 + h\nu \rightarrow h^+ + e^- \qquad (h^+ + e^- = \text{electron-hole pair}) \qquad (1)$$

In the presence of O_2

$$O_2 + e^- \rightarrow O_2^{\bullet -} \qquad (2)$$

Methanol and methoxy species adsorbed (CH_3O) on the catalyst surface can react directly with the "h^+" holes as already reported in the literature [28,29] :

$$CH_3O^- (CH_3O_{(a)}) + h^+ \rightarrow CH_3O^{\bullet} \qquad (3)$$

$$CH_3O^{\bullet} \rightarrow CH_2O^{\bullet -} + H^+ \qquad (4)$$

$$CH_2O^{\bullet -} \rightarrow H_2CO + e^- \qquad (5)$$

In the presence of $O_2^{\bullet -}$ formaldehyde could be oxidized into CO_2 and H_2O (photocombustion):

$$H_2CO + O_2^{\bullet -} \rightarrow CO_2 + H_2O + e^- \qquad (6)$$

CH_3O and CH_3OH can be oxidized to form bidentate formate species HCOO:

$$H_3O + O_2^{\bullet -} \rightarrow HCOO + H_2O + e^- \qquad (7)$$

HCOO in presence of $CH_3O^{\bullet}$ leads to the formation of methyl formate:

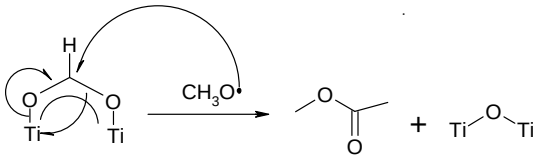

(8)

HCOO in presence of CH_3OH leads to the formation of formic acid and methoxyl radical:

$$HCOO^{\bullet} + CH_3OH \rightarrow CH_3O^{\bullet} + HCOOH \qquad (9)$$

< Figure 14 here>

UV-intensity effect

Figure 15 presents methanol (5040 ppm) photooxidation at RT on TNTs, increasing with UV-irradiation intensity (under the same condition as above). Methanol conversion was complete at intensity higher than 3.5 mW/cm^2. The selectivity was also affected by intensity: complete photocombustion was obtained at higher than 5 mW/cm^2. These results could be explained by the increase of the production of oxidant species when intensity increased. It is noteworthy that a high amount of carbonyl species was always detected in the first period of irradiation (whatever the intensity, Figure II, supplementary information). It could be assigned to the high concentration of methanol in the gas phase due to desorption phenomena mentioned above (decrease of [oxydants]/[methanol] ratio). Therefore, an increase of UV-irradiation intensity led to an increase of activity and CO_2-selectivity of the photocatalyst.

< Figure 15 here>

n-hexane photooxidation and temperature

n-hexane photooxidation was performed under the same condition as for methanol and the concentration used was 5040 ppm. The UV intensity (I_0) used was ~2 mW/cm^2. The influence of temperature on n-hexane conversion and on CO_2 production is presented in Figure 16. Once more TNTs showed higher activity than TiO_2-P25 for n-hexane photodegradation (~1.5 times, Table 2). A significant decrease of n-hexane conversion was observed with the increase of temperature (Figure 15). Only CO_2 and H_2O were observed in the gas phase (Figure III-supplementary material). This selectivity confirms that carbonyl species observed in methanol photooxidation were produced from the bidentate formate species.

< Figure 16 here>

Figure 17 presents the evolution of the IR spectra of the photocatalyst surfaces before and during n-hexane photooxidation at different temperatures. After UV irradiation, an important decrease of CH band has been noted due to desorption phenomena and photooxidation of n-hexane. No adsorption of n-hexane was observed on the hydrophilic TiOH sites. After UV irradiation, the TiOH band has disappeared, perturbed by H-bonding with newly formed hydrophilic species as confirmed by an increase of a broad band at 3660-3000cm^{-1}. In addition, new IR-bands were visible at 1800-1500 cm^{-1}, ascribed to the adsorption of carbonyl species and unsaturated hydrocarbons. These new bands increased with temperature, whereas the H-bonding seemed to decrease (with no corresponding increase of TiOH IR-band). The formation (and chemisorption) of carbonyl and unsaturated hydrocarbons is favored by heating, resulting in poisoning of the photocatalyst surface (photos of TNTs-pellets before and after photooxidations are presented in Figure IV in supplementary materials). The low increase in CO_2 production at temperatures between 45 and 75°C (Figure 16) is assigned to the incomplete photooxidation of species adsorbed on TiO_2 (n-hexane conversion decreased

in this temperature range). The increase of the UV intensity from 2 to 3.5 mW/cm^2 led to an increased photooxidation. For I_0>3.5 mW/cm^2, no significant effect has been observed, showing that residual species on the photocatalyst were poisoning the surface rather than filtering UV light.

< Figure 17 here>

Carbon monoxide photooxidation

Intensity effect

The photooxidation of 1000 ppm of CO was performed at room temperature at various UV intensities under the same flow conditions as previously. Results are presented in Figure 18. TNTs showed again higher activity than TiO_2-P25 (1.5-2 times). These results were in good agreement with CO_2 production.

< Figure 18 here>

Concentration effect

The influence of CO concentration on photooxidation at ~11 mW/cm^2 is presented in Figure 19. CO conversion decreased with increasing CO concentrations. TNTs were again more active than TiO_2-P25 (Table 2) and the difference was higher when the CO concentration was lower.

< Figure 19 here>

< Table 2 here>

Conclusion

Operando-IR proved to be the ideal technique to study photocatalytic air purification. Coupling this technique to on line analysis (gas-IR and MS) allowed real time monitoring of the species adsorbed on the surface of the photocatalyst and of those formed in the gas phase. Using self supporting photocatalyst wafers and homogenous irradiation gives access to the activity, selectivity and mechanism of the process. Different parameters could be changed (temperature, VOC concentration…) and their influence on the photocatalysis reaction was evaluated. In order to demonstrate the reliability of this technique, two photocatalyst were studied in this work; TiO_2-nanotubes (TNTs) as new photocatalyst and TiO_2-P25 as reference. The IR characterization of TNTs and TiO_2-P25 allowed understanding the role of surface TiOH groups in the reaction. Our results indicate an influence of the amount of TiOH groups on the TiO_2 band gap. On the other hand, these sites (especially Ti(IV)OH sites) improve chemisorption of (hydrophilic) methanol and favors its photooxidation. The photooxidation of methanol, n-hexane and carbon dioxide using TNTs and TiO_2-P25 was performed. TNTs was 1.5 to 2 times more active and selective than TiO_2-P25 in methanol photooxidation, with improved results at higher temperature and UV-irradiation intensity or at lower methanol concentration. A negative influence of temperature was observed for n-hexane photooxidation, assigned to surface poisoning by unsaturated species (coke). TNTs material were also more active and selective than TiO_2-P25 for photooxidation of CO into CO_2, with a negative influence of CO concentration. As conclusion, TNTs material were generally more active and selective than the reference TiO_2-P25 because of higher surface area.

Acknowledgement

The authors wish to thank Prof. S. Bals and Ms. J. Pauwels from EMAT, physics department of the University of Antwerp, Belgium, for recording the TEM picture of TNT.

Graphical abstract

New operando-IR techniques to study the photocatalytic activity and selectivity of TiO_2-nanotubes in air purification: influence of temperature, UV intensity and VOC concentration.

Mohamad El Roz, Monika Kus, Pegie Cool, Frederic Thibault-Starzyk

A new operando-IR technique has been used to investigate the photocatalytic activity and selectivity of TiO_2-nanotubes. Real time IR-monitoring of the photocatalyst surface (identification of surface species) and of the gas phase of the reaction (products identification) gives access to the reaction mechanism and photocatalyst activity and selectivity. Coupling this technique with mass spectrometry gave complementary information on the gas phase during the photocatalytic reaction. The possibility to change and control several parameters (VOCs concentration, UV-intensity and temperature…) led to understand their influence on the reaction, showing the interest of operando-IR technique in photocatalysis studies. TiO_2-nanotubes were always more active and selective than the reference TiO_2-P25.

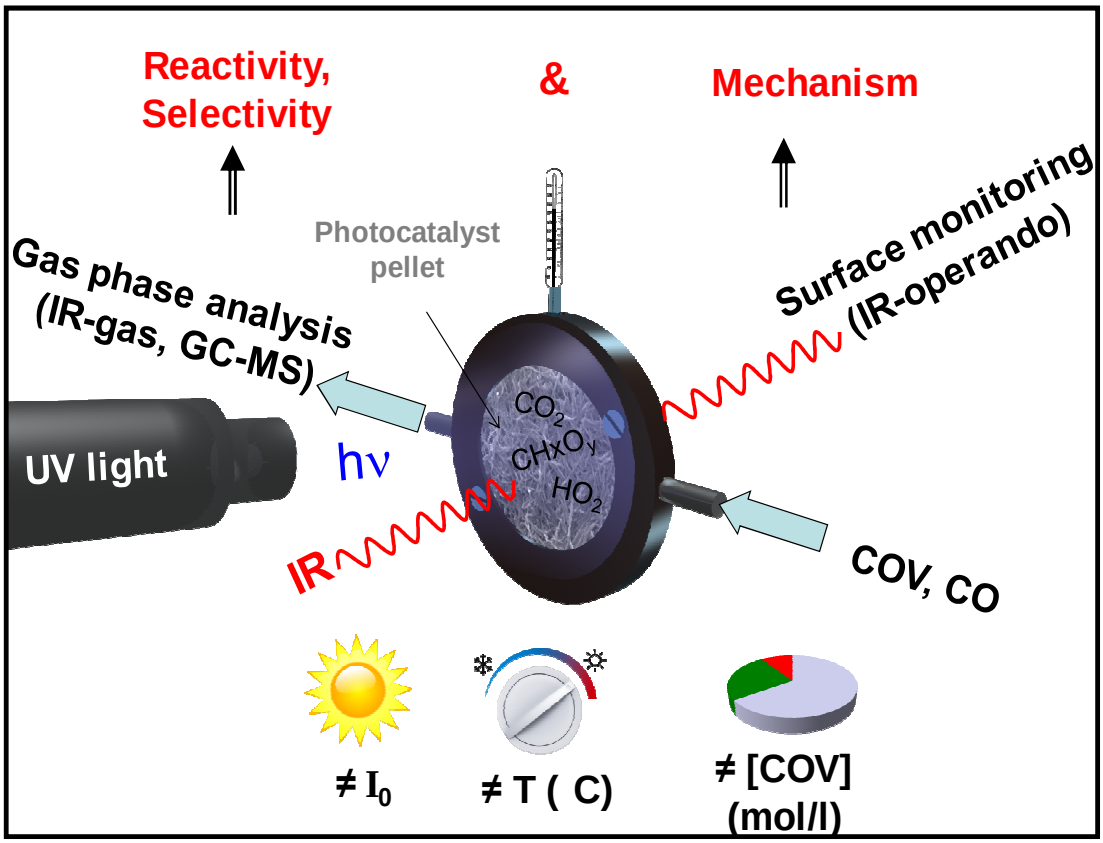
Reactivity,
Selectivity
&
Mechanism
Photocatalyst
pellet
Gas phase analysis
(IR-gas, GC-MS)
Surface monitoring
(IR-operando)
UV light
hν
IR
CO_2
$CHxO_y$
HO_2
COV, CO
≠ I_0
≠ T (C)
≠ [COV]
(mol/l)

Tables

Table 1. Height of TiOH IR-bands and area bands of pyridine adsorbed on the TNTs and TiO_2-P25 surfaces (per 10 mg/cm^2 of sample).

	band heigth (a.u.)		band area (cm^{-1})			
band (cm^{-1})	3720 cm^{-1}	3690 cm^{-1}	1610 cm^{-1}	1575 cm^{-1}	1491 cm^{-1}	1448 cm^{-1}
TNTs	0,13	0,164	3	0,22	0,44	2,8
TiO2	0,10	0,062	2,1	0,14	0,28	1,1
ratio	1,3	2,65	1,4	1,6	1,57	2,5

Table 2. Reactivity and selectivity of methanol, n-hexane and carbon dioxide photooxidation reactions using TNTs and TiO_2-P25 as photocatalysts. (Conv.= conversion; Select. = selectivity.)

I_0 ~2 mW/cm^2	T (°C)	Photooxidation of				
		Methanol		n-hexane		CO
photocatalyst		Conv. (%)	CO_2-select. (%)	Conv. (%)	CO_2-select. (%)	Conv. (%)
TNTs	30	30%	85%	23%	100%	25%
	200	75%	60%	5%	100%	-
TiO_2-P25	30	14%	47%	12%	100%	10%
	200	56%	44%	2%	100%	-

Figure captions

Figure 1. SEM pictures of TiO_2-P25 (a) and TNTs powders. "(c)" correspond to the TEM picture of TNTs powders.

Figure 2. XRD results of TiO_2-rutile (a) TiO_2-P25 (b) TiO_2-nanotube after calcination (c) and TiO_2 nanotube before calcination (d).

Figure 3. Raman results of TiO_2-nanotube after calcination (a) and TiO_2-nanotube before calcination (b).

Figure 4. N_2-sorption isotherms of TNTs and TiO_2-P25 samples.

Figure 5. UV-Vis DR spectra of TiO_2-P25 (a) TiO_2-nanotube after calcination (b) and TiO_2 nanotube before calcination (c).

Figure 6. IR spectra of TiO_2-P25 (a) and TNTs (b) under air at RT (1) and after activation under vacuum at 200°C (2) (spectra collected after cool down to RT).

Figure 7. (A) Subtraction results of IR spectra of TiO_2-P25 (a) and TNTs (b) after pyridine adsorption and evacuation under vacuum at 200°C (subtraction from the IR spectra of the photocatalysts after activation and before pyridine adsorption). **(B)** Evolution of the IR-bands height of TiOH bonds vs. temperature after pyridine adsorption.

Figure 8. (A) Evolution of TNTs IR spectra during the methanol adsorption. **(B)** IR spectra of TNTs (a) and TiO_2-P25 (b) after methanol saturation.

Figure 9. The IR spectra vs. time (and temperature) of the gas phase during the photooxidation of methanol at different temperatures using the TNTs **(A)** and TiO_2-P25 **(B)** as photocatalyst: The flask corresponds to the turn-on time of the UV-lamp.

Figure 10. IR-gas spectra of the methanol photooxidation reaction before (a) and during (b) irradiation. (c), (d) and (e) correspond to the IR-gas spectra of formaldehyde, methyl formate and formic acid respectively.

Figure 11. Evolution of the methanol conversion vs. temperature (a) and CO_2 selectivity (b), determined using IR spectra of the gas phase, during the methanol photooxidation using TNTs (A) and TiO2-P25 (B) as photocatalysts. ([MeOH]=5040ppm, I_0~2mW/cm2, Flow=25 cm^3/min).

Figure 12. Evolution of the methanol conversion (calculated using the m/z=31 MS signal) and MS signal of H_2O (m/z=18) (b) and CO_2 (m/z=44) (c) at different temperatures during the methanol photooxidation.

Figure 13. IR-gas **(A)** and MS **(B)** results obtained during the methanol photooxidation at different temperatures: methanol conversion (a) and (b) CO_2 selectivity.

Figure 14. IR spectra of the TNTs **(A)** and the gas phase **(B)**, before (a) and during irradiation at RT (b) and 120°C (c).

Figure 15. (A) Effect of the UV lamp intensities on the methanol conversion (square) and on CO_2 (circle) and carbonyl species (diamond) production determined using IR spectra of the gas phase. **(B)** Original IR spectra of the gas phase during the photooxidation of methanol at different intensities of the UV-lamp at RT temperature.

Figure 16. Evolution of the n-hexane conversion vs. temperature (determined using the IR-gas spectra) and CO_2 IR-band area, during the n-hexane photooxidation using TNTs **(A)** and TiO_2-P25 **(B)** as photocatalysts. ([n-hexane] = 5040ppm, I_0 ~2mW/cm^2, Flow = 25 cm^3/min).

Figure 17. (A) Evolution of the IR spectra of TNTs (I) and TiO_2-P25 (II) vs temperature during the photooxidation of n-hexane. **(B)** Subtraction results of the IR spectra of TNTs (I) and TiO_2-P25 (II) during the photooxidation of n-hexane at RT (a) and 200°C (b), from the IR spectrum before UV irradiation. (I_0~ 2mW/cm^2; [n-hexane] = 5040 ppm; 20%O_2/Ar, flux=25 cm^3/min).

Figure 18. (A) Evolution of the CO photooxidation (close symbol) and CO_2 production (open symbol) vs lamp intensities using TiO_2-P25 (square) and TNTs (circle) as photocatalysts. Figure **(B)** corresponds to the CO_2 evolution in real time at different intensities.

Figure 19. Evolution of the CO photooxidation vs. the CO concentration using TiO_2-P25 (square) and TNTs (circle) as photocatalysts. I_0 = 2 mW/cm^2.

Figures

Figure 1

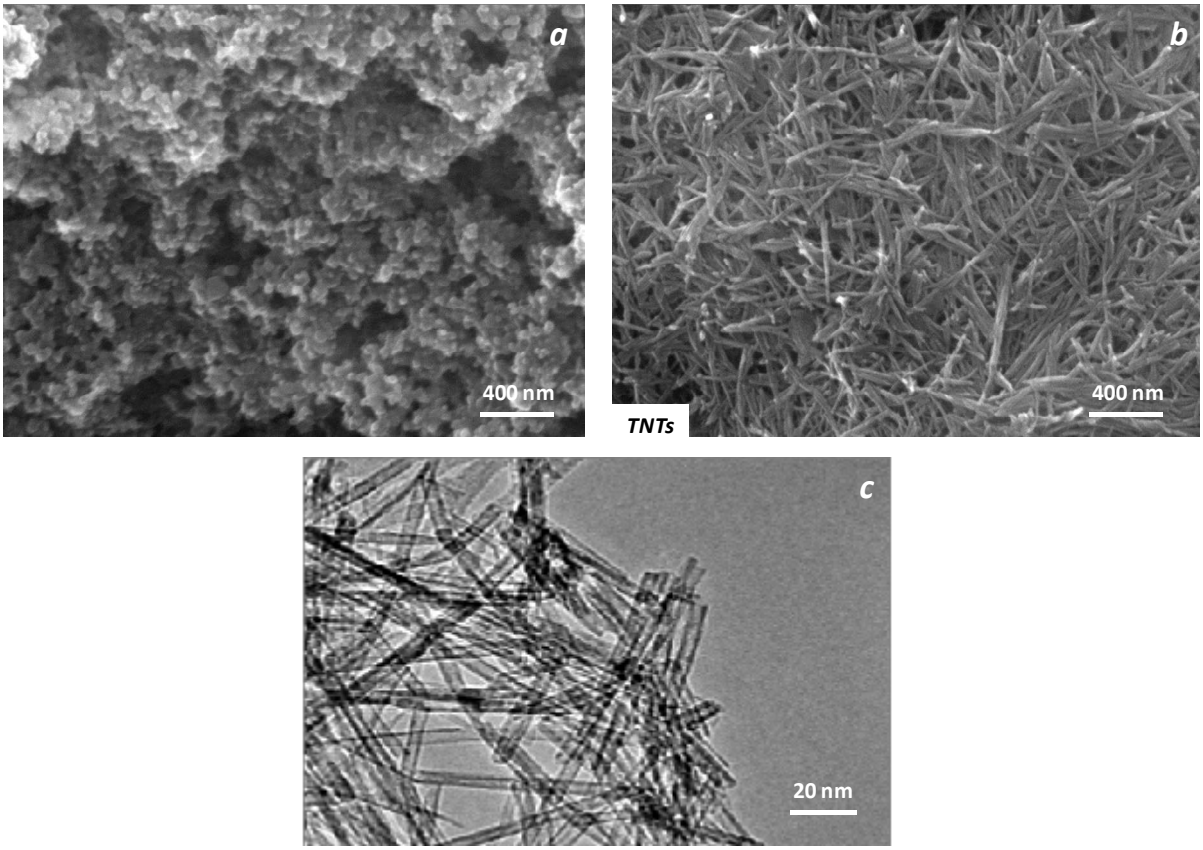

Figure 2

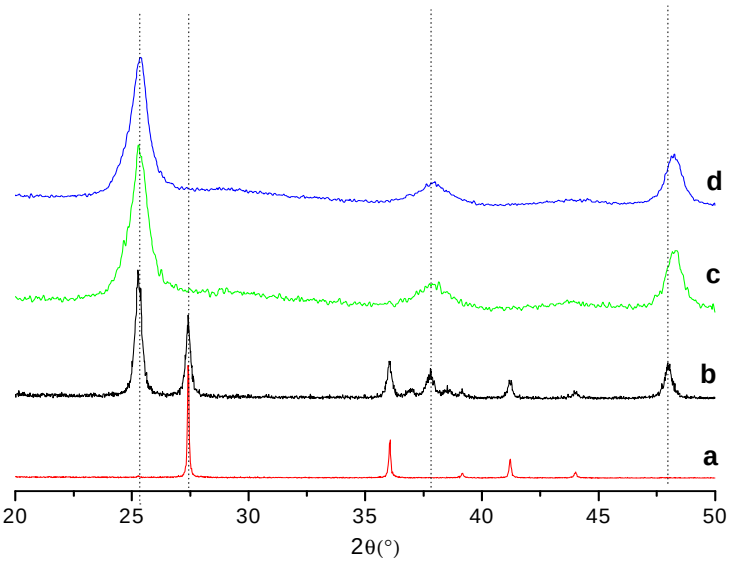

Figure 3

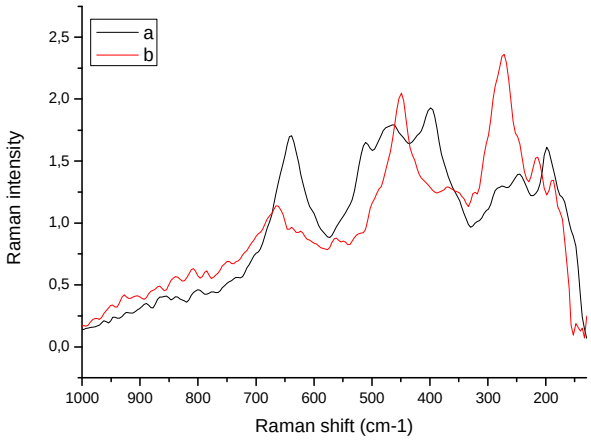

Figure 4

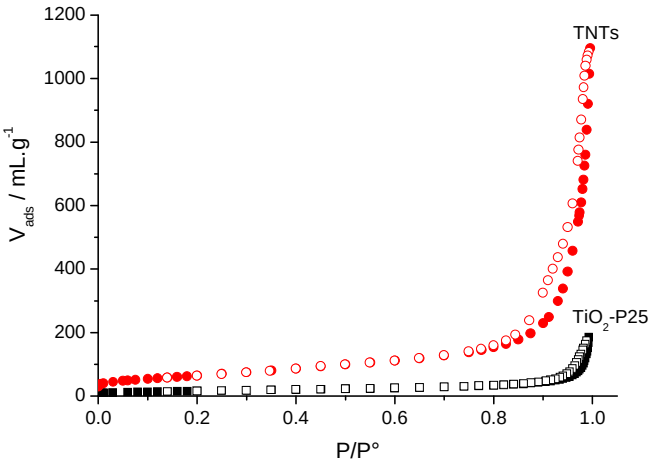

Figure 5

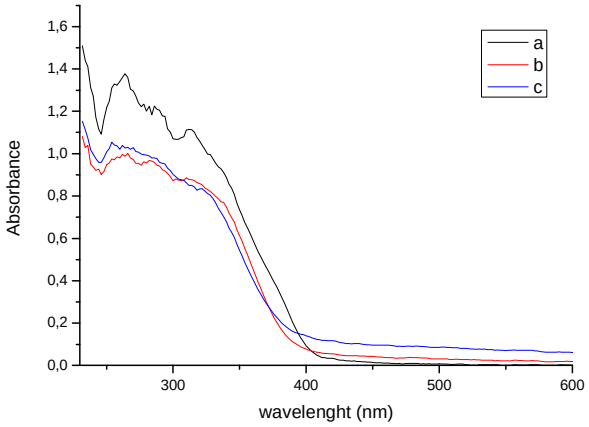

Figure 6

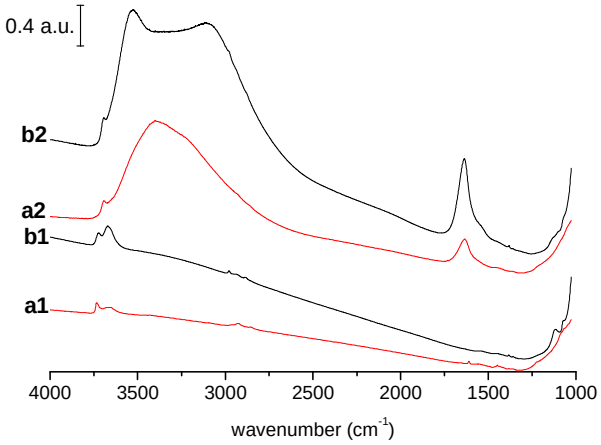

Figure 7

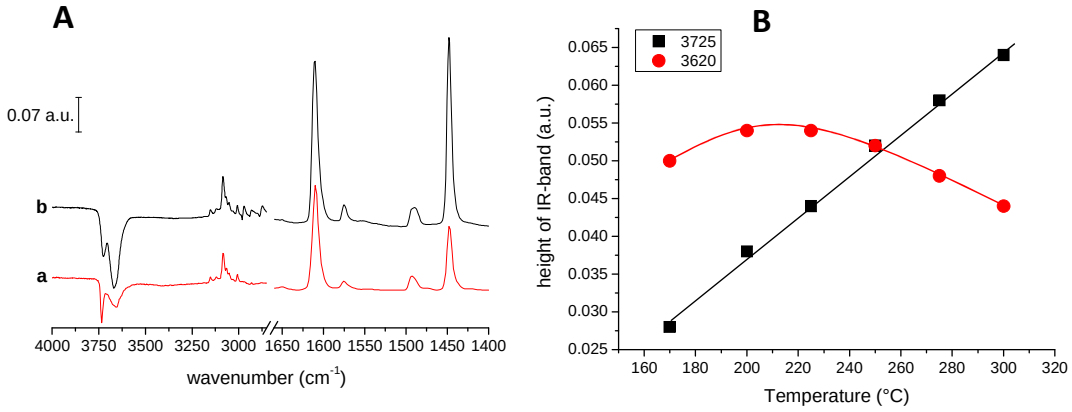

Figure 8

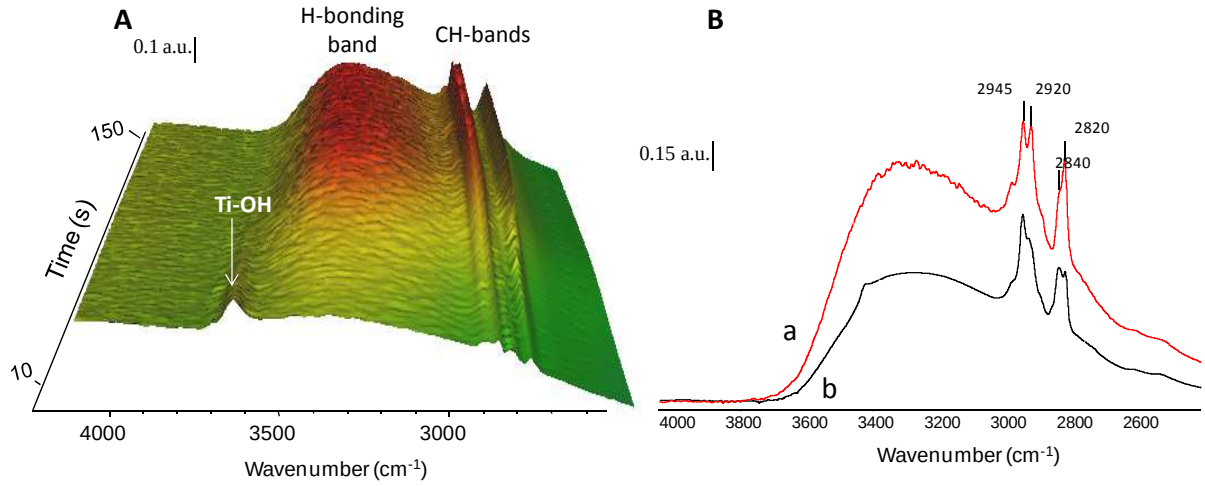
A
0.1 a.u.
H-bonding band
CH-bands
150
Time (s)
Ti-OH
10
4000
3500
3000
Wavenumber (cm-1)
B
0.15 a.u.
2945
2920
2820
2840
a
b
4000
3800
3600
3400
3200
3000
2800
2600
Wavenumber (cm-1)

Figure 9

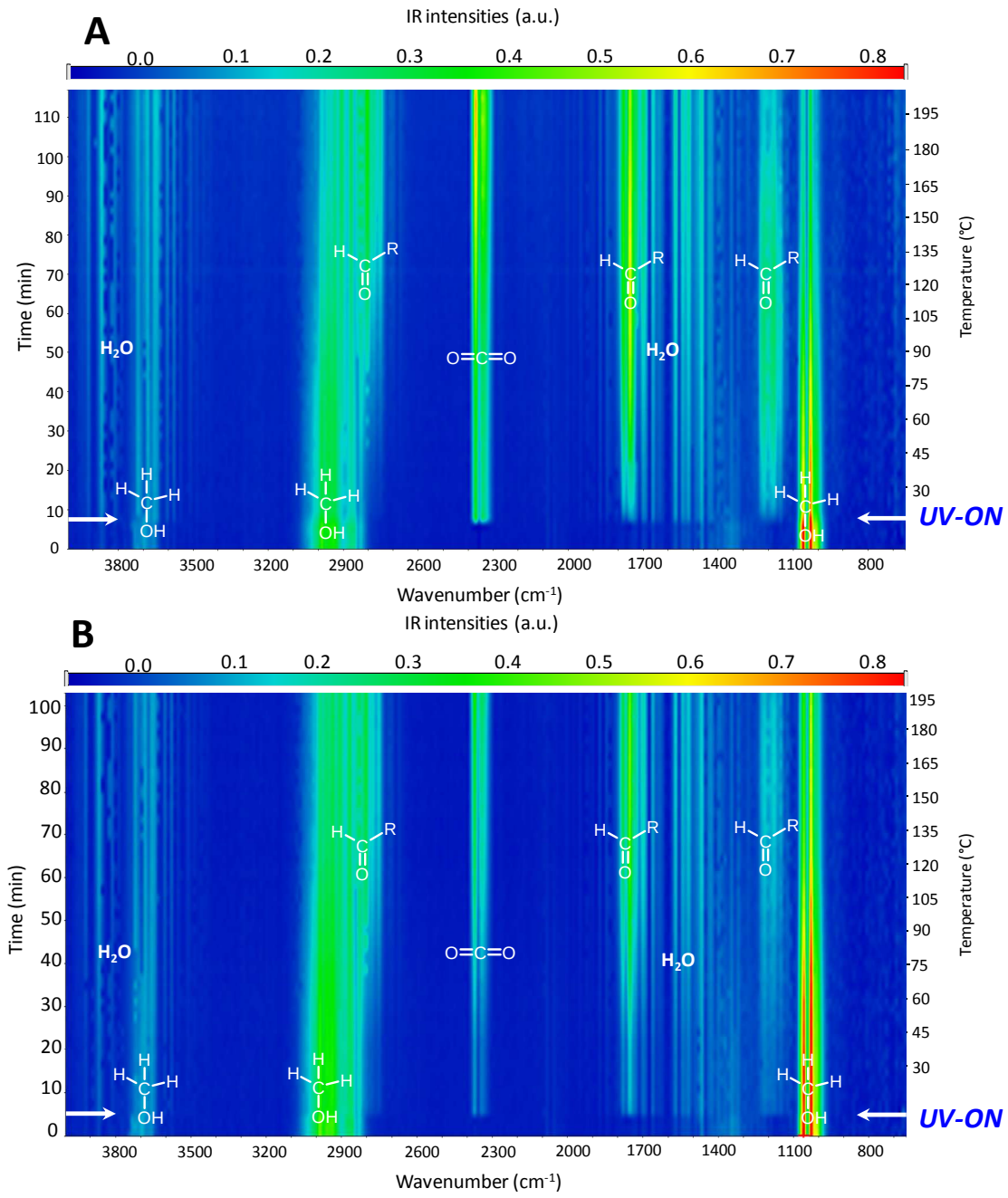
A
IR intensities (a.u.)
0.0
0.1
0.2
0.3
0.4
0.5
0.6
0.7
0.8
Time (min)
Temperature (°C)
H2O
O=C=O
H2O
UV-ON
Wavenumber (cm-1)
3800
3500
3200
2900
2600
2300
2000
1700
1400
1100
800
B
IR intensities (a.u.)
Time (min)
Temperature (°C)
H2O
O=C=O
H2O
UV-ON
Wavenumber (cm-1)

Figure 10

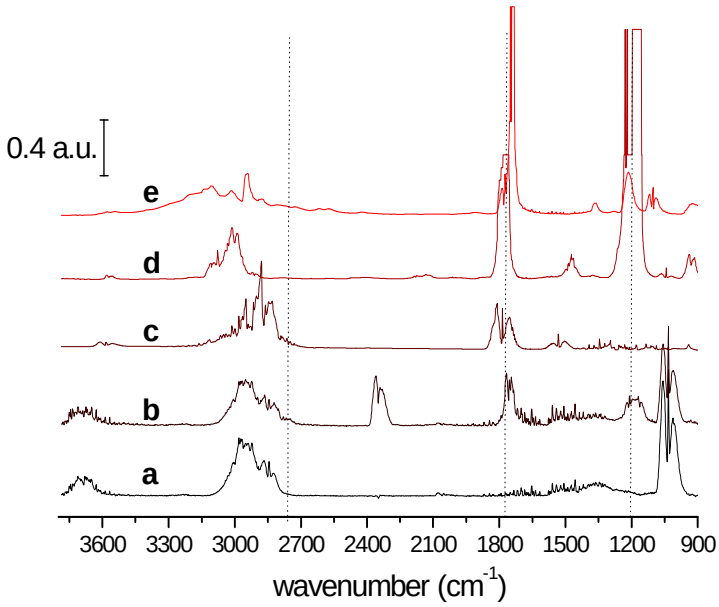

Figure 11

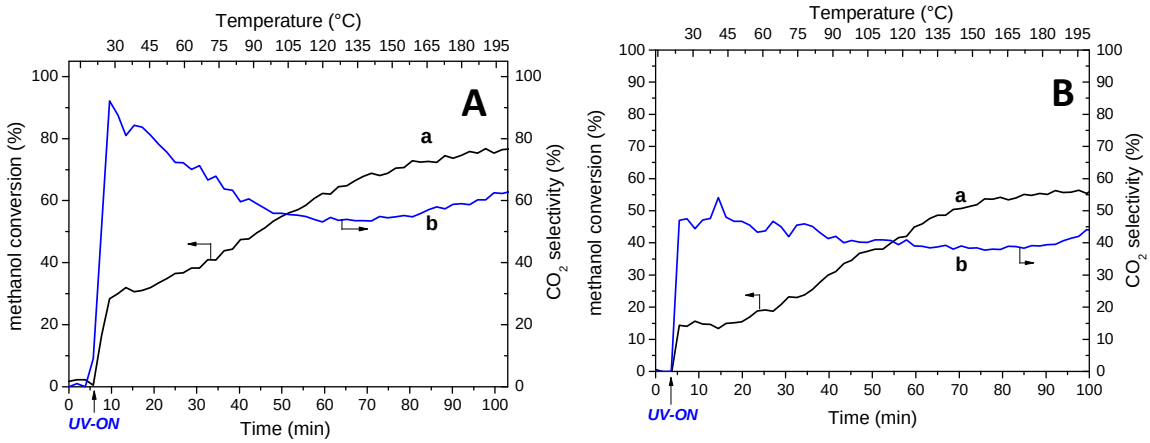

Figure 12

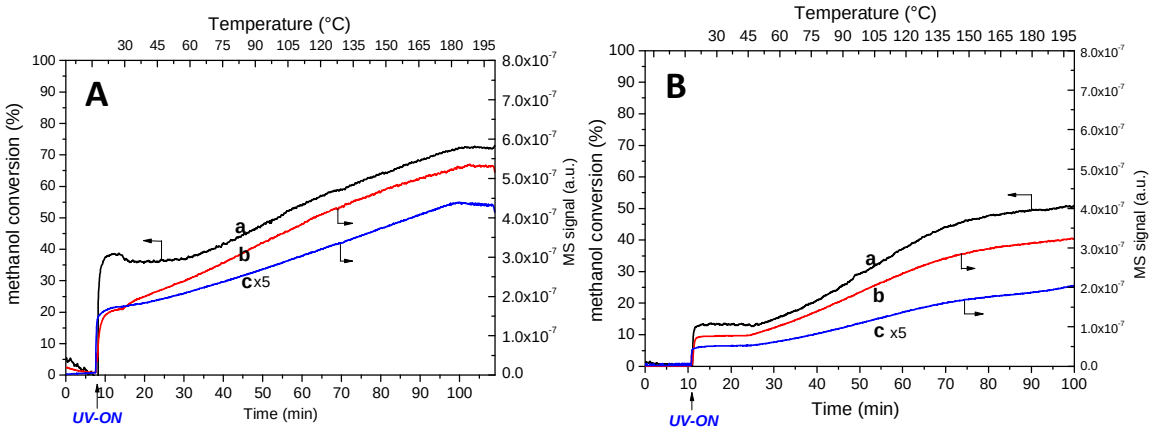

Figure 13

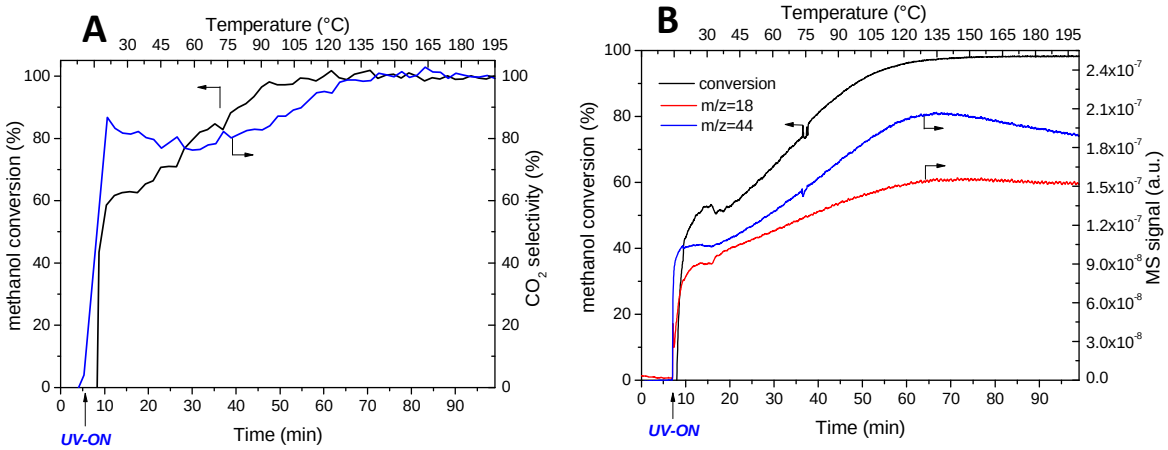

Figure 14

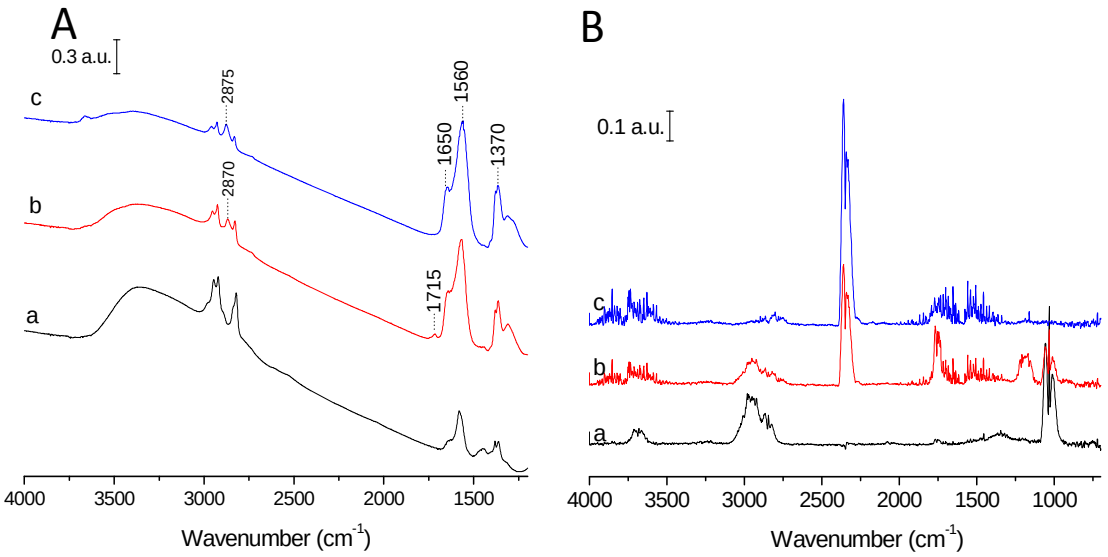

Figure 15

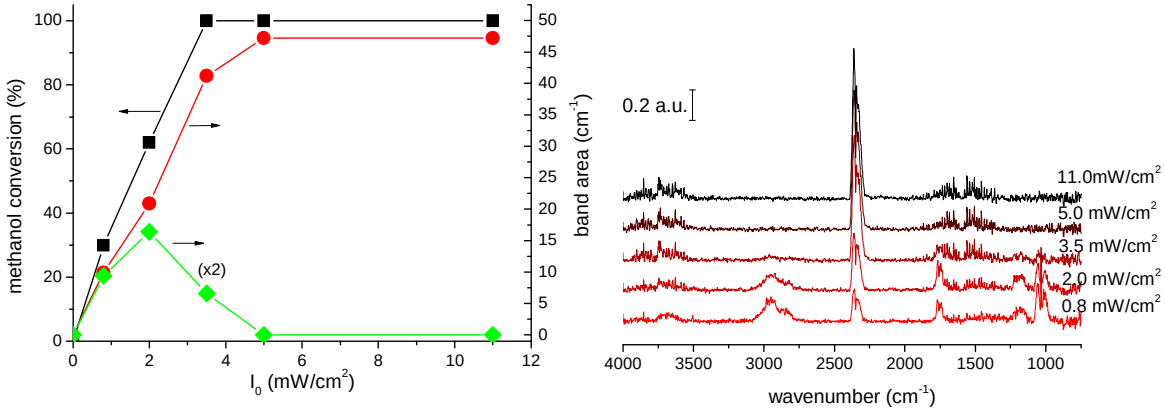

Figure 16

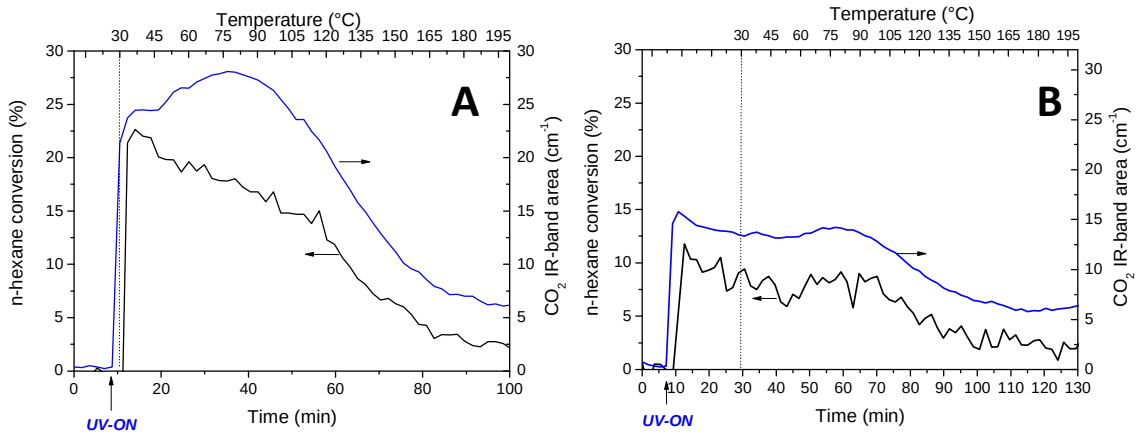

Figure 17

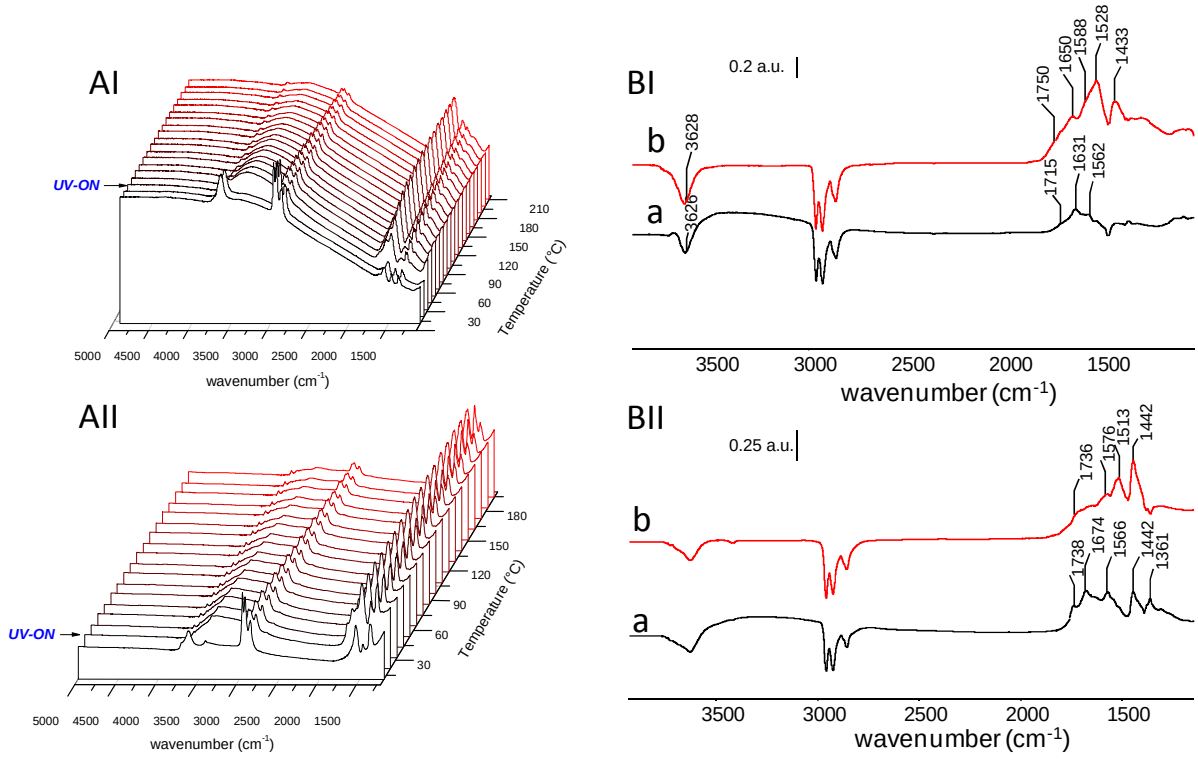

Figure 18

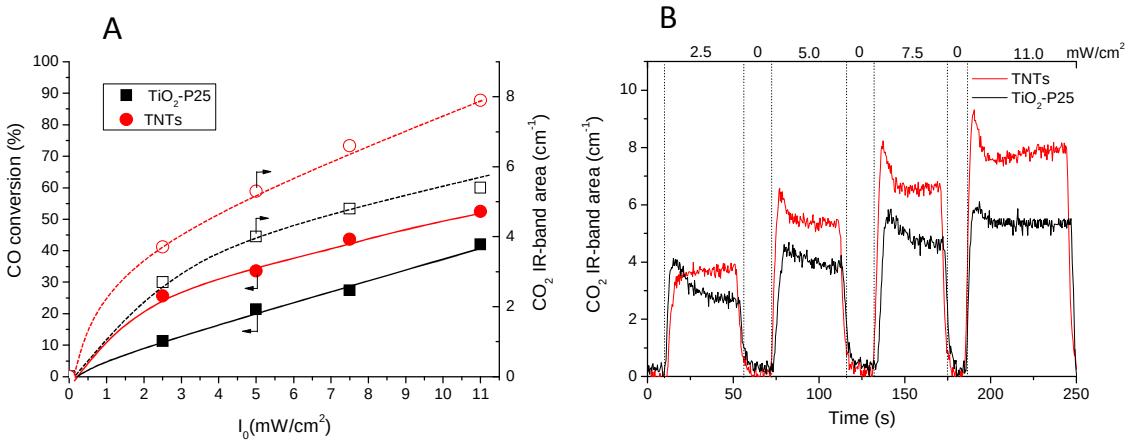

Figure 19

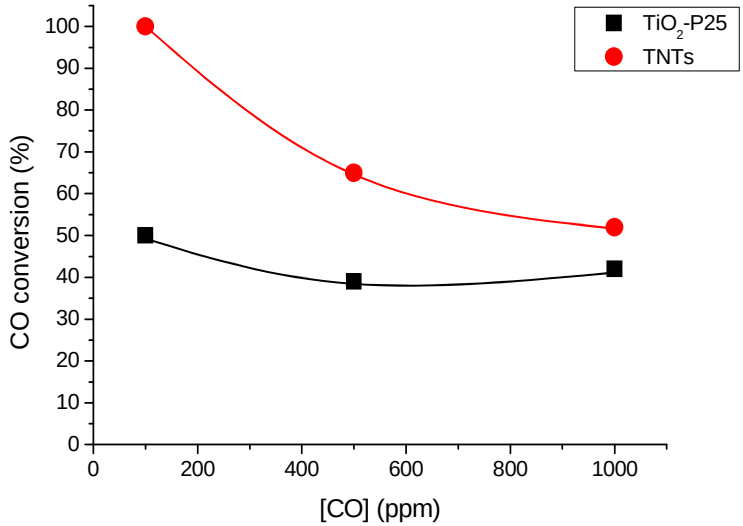

Reference

[1] O'Regan, B.; Graetzel, M. *Nature* **1991**, *353* 737–740.

[2] Ghicov, A.; Tsuchiya, H.; Hahn, R.; Macak, J. M.; Munoz, A.G.; Schmuki, P.; *Electrochem. Commun.* **2006**, *8,* 528–532.

[3] Fujishima, A.; Hashimotoand ,K.; Watanabe, T. *TiO_2 Photocatalysis. Fundamentals and Applications*; BKC, Inc.: Tokyo, **1999**.

[4] Macak, J. M.; Zlamal, M.; Krysa J.; Schmuki, P. *Small* **2007**, *3*, 300–304.

[5] Matthews, R.W. *J. Phys. Chem*. **1987**, *91*, 3328–3333.

[6] Robertson, J.M.C.; Robertson P.K.J.; Lawton, L.A. *J. Photochem. Photobiol. A: Chem.* **2005**, *175*, 51–56.

[7] Macak, J.M.; Tsuchiya, H.; Ghicov, A.; Yasuda, K.; Hahn, R.; Bauer, S.; Schmuk, P. *Curr.Opin. in Solid State and Mater. Sci.* **2007**, *11*, 3–18.

[8] Ghicov, A.; Schmuki, P. *Chem. Commun.* **2009**, 2791–2808.

[9] Zhang, Z .; Yuan , Y.; Shi , G.; Fang , Y.; Liang, L.; Ding , H.; Jin, A.L. *Environ. Sci. Technol.* **2007**, *41*, 6259–6263.

[10] Ribbens, S.; Meynen, V.; Van-Tendeloo, G.; Key, X.; Mertens, M.; Maes, B.U.W.; P. Cool, Vansant, E.F. *Micro. Meso. Mater.* **2008**, *114*, 401–409.

[11] EL-ROZ, M. ; L. Lakiss, Valtchev, V. ; Mintova, S., Thibault-Starzyk, F. *Micro. Meso. Mater.* In press, DOI: 10.1016/j.micromeso.2012.03.003.

[12] Lesage, T.; Verrier, C.; Bazin, P.; Saussey J.; Daturi, M. *Phys. Chem. Chem. Phys.* **2003**, *5*, 4435–4440.

[13] Chuang, C.C.; Wu, W.C.; Huang, M.C.; Huang, I.C.; Lin, J.L. *Journal of Catalysis* **1999**, *185*, 423–434.

[14] Thibault-Starzyk, F.; Vimont A.; Gilson, J.P. *Catal. Today* **2001**, *70*, 227–241.

[15] Szczepankiewicz, S.H.; Moss, J.A.; Hoffman, M.R. *J. Phys Chem. B*, **2000**, 104, 9842–9850.

[16] Wu, N.; Lee, M.S.; Pon, Z.J.; Hsu J.Z. *J. Photochem. Photobiol. A: Chem.* **2004**, *163*, 277–280.

[17] Balcerski, W.; Ryu, S.Y.; Hoffman, M.R. *Intern. J. Photoenerg*. **2008**, *2008*, 1–9.

[18] Wu, B.; Yuan, R.; Fu, X.; *J. Sol. St. Chem.* **2009**, *182*, 560–565.

[19] Zaki, M. I.; Hasan, M. A.; Al-Sagheer, F. A.; Pasupulety, L. *Colloids Surf. A* **2001**, *190*, 261–274.

[20] Wang, X.; Kim, S.; Buda, C.; Neurock, M.; Koper, O. B.; J.T. Yates, Jr. *J. Phys. Chem. C* **2009**, *113*, 2228–2234.

[21] Chuang, C.C.; Chen C.C.; Lin, J.L. *J. Phys. Chem. B* **1999**, *103*, 2439–2444.

[22] Lavalley, J.C.; Sheppard, N.; *Spectrochim. Acta* **1972**, *28*, 2091–2101.

[23] Busca, G.; Elmi A.; Forzatti, P.; *J. Phys. Chem.* **1987**, *91*, 5263–5269.

[24] Lochar, V. *Appl.Cata. A: General* **2006**, *309*, 33–36.

[25] Popova, G.Y.; Andrushkevich, T.V.; Chesalov, Y.A. ; Stoyanov, E.S. *Kinetics and Catalysis*, **2000**, *41*, 805–811.

[26] Arana, J.; Dona-Rodriguez, J.M.; Garrigai Cabo, C.; Gonzalez-Diaz, O.; Herrera-Melian J.A.; Perez-Pena, J. *Applied Catalysis B: Environmental* **2004**, *53*, 221–223.

[27] Arana, J.; Dona-Rodriguez, J.M.; Garrigai-Cabo, C.; Gonzalez-Diaz, O.; Herrera-Melian J.A.; Perez-Pena, J. *Applied Surface Science* **2004**, *239*, 60–71.

[28] Buzzoni, R.; Bordiga, S.; Ricchiardi, G.; Lamberti, C.; Zecchina A.; Bellussi, G. *Langmuir* **1996**, *12*, 930–940.

[29] Yamakata, A.; Ishibashi T.; Onishi, H. *Int. J. Photoenergy* **2003**, *5*, 7–9.